

# A prismatic approach to describe the hysteretic behavior of smart materials: An application to shape memory alloys

Journal of Intelligent Material Systems and Structures  
2025, Vol. 36(9) 563–578  
© The Author(s) 2025  
Article reuse guidelines:  
sagepub.com/journals-permissions  
DOI: 10.1177/1045389X251332432  
journals.sagepub.com/home/jim



Vanderson M Dornelas<sup>1</sup>, Sergio A Oliveira<sup>2</sup> and Marcelo A Savi<sup>1</sup> 

## Abstract

Hysteretic response of smart materials has complex mathematical modeling. Thermodynamic-based constitutive models belong to an important class of models and data-driven models are interesting alternatives that avoid complex algorithms and parameter determinations. The classical Preisach model describes multidisciplinary hysteretic behavior employing mathematical operators in a triangular domain. The Everett function is an alternative build a surface from experimental data, replacing the original integral form to a summation. This paper proposes a novel approach, extending the Preisach triangular domain to a prismatic domain that allows a broader description of distinct phenomena. The idea is to use the Preisach approach for different triangles and then performing an interpolation for a prismatic domain, enabling the representation of distinct phenomena that, otherwise would not be described. Shape memory alloys (SMAs) are employed as a representative example of smart materials. Experimental tests are developed in order to define reference cases to be analyzed. Numerical simulations are carried out and compared with experimental data, evaluating the model capabilities under different loading conditions. Specifically, temperature-dependent and cyclic-dependent behaviors are of concern. The results show the model ability to describe the general thermomechanical behavior of shape memory alloy hysteretic behavior, being in close agreement with experimental data.

## Keywords

Shape memory alloys, hysteresis, Preisach model, Everett function, experimental analyses, numerical simulations

## 1. Introduction

The increasing demand for innovative technologies has driven research and development of materials that actively interact with the environment. Smart, adaptive, or active materials have as the main characteristic the ability to adapt to the environment due to multiphysical couplings that connect different physical domains such as mechanical, electrical, thermal, magnetic, among others.

The complex multidisciplinary behavior of smart materials is associated with hysteretic characteristics described by complex mathematical models. The constitutive modeling deals with the macroscopic behavior, presenting a thermodynamic-based phenomenological description. On this basis, numerical procedures are usually employed together with a challenging determination of model parameters. Data-driven models present a generalist perspective for the description of different phenomena. The hysteresis models are experimental-driven descriptions, being adjusted through geometric perspectives with the advantage of simple numerical implementation when compared to classical thermodynamic-based models.

The Preisach model is a well-established alternative for describing hysteresis in smart materials (Khandelwal and Buravalla, 2009; Wang et al., 2007). Initially proposed to deal with the hysteretic behavior of ferromagnetic materials (Preisach, 1935), it establishes a framework to describe hysteretic phenomena from mathematical operators defined within a triangular domain. Mayergoyz (1991, 2003) proposed an alternative formulation of the Preisach model that utilizes Everett functions derived from experimental data, replacing the original integral form to a summation.

<sup>1</sup>Center for Nonlinear Mechanics, COPPE - Mechanical Engineering, Universidade Federal do Rio de Janeiro, Rio de Janeiro, Brazil

<sup>2</sup>Department of Mechanical Engineering, CEFET/RJ - Centro Federal de Educação Tecnológica Celso Suckow da Fonseca, Rio de Janeiro, Brazil

Data Availability Statement included at the end of the article

### Corresponding author:

Marcelo A Savi, Center for Nonlinear Mechanics, COPPE - Mechanical Engineering, Universidade Federal do Rio de Janeiro, P.O. Box 68.503, Rio de Janeiro - RJ, 21941-972, Brazil.  
Email: savi@mecanica.coppe.ufrj.br

The use of Preisach model to describe piezoelectric materials were discussed by Song et al. (2005), Dong et al. (2014), Xue et al. (2017), and Sun et al. (2024). Magnetic shape memory alloys were studied by Sordon et al. (2024). Additionally, magnetostrictive materials were addressed by Davino et al. (2004), Li et al. (2013), Trapanese et al. (2014), Labusch et al. (2019), Hossain et al. (2023) and Gao et al. (2024).

Concerning shape memory alloys (SMAs), Smith (2005) presented a discussion about the application of the Preisach model for SMA modeling. Hughes and Wen (1995, 1997) identified the microstructural mechanisms responsible for hysteresis in both shape memory alloys and piezoelectric materials, highlighting the similarities between the hysteresis of these materials. Gorbet et al. (1998) performed numerical-experimental comparisons using the Preisach model using experimental data from an SMA wire-based actuator indicating a good agreement with experimental data. Khan and Lagoudas (2002) investigated the description of pseudoelastic SMA spring behavior employed in vibration absorbers. Rao and Srinivasa (2013) proposed a hybrid model to describe the pseudoelastic response for SMA wires and springs (Doraiswamy et al., 2011). Rao et al. (2014) investigated the response of pseudoelastic SMA wires subjected to torsional loads with subloops through experimental tests. Chen et al. (2019) proposed a discrete Preisach model to explore the use of SMAs in aircraft morphing wings.

Alvares et al. (2024) analyzed the thermomechanical behavior of shape memory alloys using the Preisach model based on the Everett function derived from experimental data. Results show that the model can reproduce the main macroscopic features of SMA thermomechanical behavior, properly describing stress-strain, strain-temperature, and force-displacement curves for different SMA elements as wires and springs. Distinct phenomena were discussed showing the model ability to deal with SMA macroscopic behaviors, including internal subloops. Liu et al. (2023) proposed a temperature-displacement hysteresis model based on the Preisach model for the displacement control of an SMA-based actuator. The integration of a PID control with the hysteresis model allowed precise management of the structure's deformation.

Semenov et al. (2024) proposed an overview of the main contributions of the recent years focusing on different dynamical systems using the Preisach model for hysteresis characterization. In addition, several engineering applications of the Preisach model in fields such as energy storage devices, systems that use the piezoelectric effect, and models of shape memory systems were described. Vasquez-Beltran et al. (2021) presented a study of the use of Preisach operators for describing hysteresis behavior with multidirectional-oriented loops presented in smart materials such as

SMAs and piezoelectric materials employed as high-precision sensor and actuator systems.

This work uses the SMA as a representative example of smart materials, being adopted as a reference case of the hysteretic behavior. SMAs are smart materials with the ability to recover their shape by imposing a temperature and/or a stress field. Different thermomechanical behaviors are observed including shape memory effect, pseudoelasticity, and more complex phenomena such as transformation-induced plasticity (TRIP), phase transformation due to temperature variation, and tension-compression asymmetry. These phenomena are due to solid martensitic phase transformations that involve shear displacement of atoms on a scale smaller than the interatomic distance, resulting in significant deformations and minor volume changes (Lagoudas, 2008; Leo, 2007; Yamauchi et al., 2011).

SMAs have remarkable characteristics that make them ideal for use in a variety of applications considering different areas such as automotive (Anumodh et al., 2021; Shreekrishna et al., 2022), civil structures for vibration control (Chang and Araki, 2016; Isalgue et al., 2006; Janke et al., 2005), biomedical devices (Chaudhary et al., 2024; Elahinia, 2016; Machado and Savi, 2003; Nair and Nachimuthu, 2022; Nematollahi et al., 2019), origami-inspired systems and structures (Fonseca et al., 2022), robotics (Ruth et al., 2022; Sreekumar et al., 2007), oil & gas industry (Patil and Song, 2017), and aerospace (Leal et al., 2018; Leal and Savi, 2018; Lecce and Concilio, 2015). In addition to these contributions, a general review of the main applications and future perspectives for the use of shape memory alloys can be found in the works proposed by Mohd Jani et al. (2013) and Kumar et al. (2024).

The mathematical modeling of SMAs is associated with significant scientific and technological relevance and an overview of the most relevant models were presented by Paiva and Savi (2006), Khandelwal and Buravalla (2009), Cisse et al. (2016a, 2016b), and Chowdhury (2018). In addition, it is worth highlighting the recent contributions: Alsawalhi and Landis (2022), Adeodato et al. (2022), and He et al. (2023). Besides, it should be pointed out models dealing with complex phenomena related to SMA behavior including three-dimensional behavior (Oliveira et al., 2016; Rao et al., 2023), transformation-induced plasticity (Oliveira et al., 2018), functional and structural fatigue (Dornelas et al., 2020, 2021; Hasan and Baxevanis, 2022; Kan et al., 2023; Phillips et al., 2019).

Karakalas et al. (2019) proposed a constitutive model to describe the hardening behavior of SMAs enabling the description of internal subloops. Rizzello et al. (2018) developed a model to describe the dynamical behavior of polycrystalline SMA based on a modified version of the Müller-Achenbach-Seelecke model, properly predicting the internal subloops and loading

rate effects. Wang et al. (2021) presented a thermomechanical model for pseudoelastic shape memory alloys within a finite-strain and thermodynamical framework to describe the complex internal hysteresis effect due to incomplete phase transformation. Scalet et al. (2021) presented a three-dimensional finite strain constitutive model considering transformation-induced plasticity to describe partial phase transformation during cyclic thermomechanical loadings. Wang et al. (2022) proposed an elastoplasticity model with three coupled quantities for isotropic and anisotropic hardening to simulate the pseudoelastic effects of SMAs. Hasan et al. (2022) developed a finite-strain, phase-field model to analyze thermomechanically induced fracture in shape memory alloys, capturing fracture behavior under loading paths. Young et al. (2024) investigated fracture toughness, actuation, and mechanical fatigue crack growth responses of high-temperature shape memory alloys employing a single Paris Law Curve to estimate actuation fatigue crack growth rates to detect mechanical fatigue crack growth rates.

This paper proposes a novel prismatic approach, based on the Preisach model, for the description of hysteretic behavior of smart materials. The idea is to define a novel domain extending the classical Preisach triangle to a prismatic domain, allowing a broader description of hysteretic behaviors. The usual Preisach representation is preserved from the superposition of operators in a triangular domain, which allows the construction of the Everett surface based on experimental data. The novel dimension is accessed through interpolation between these surfaces, allowing the general description of the material behavior, incorporating the capability to describe new phenomena. The thermomechanical behavior of shape memory alloys is adopted as a representative case of smart materials due to their complex hysteretic responses. Either temperature-dependent or cyclic-dependent responses are of concern, allowing to deal with situations that the classical Preisach model is not able to describe. Quasi-static tensile tests are carried out to evaluate the stress-strain response of an SMA wire at different temperatures, and cyclic-dependent responses involving transformation-induced plasticity (TRIP; Oliveira et al., 2018). Numerical simulations are conducted to validate the model ability to describe the SMA thermomechanical behavior using the presented experimental results as reference. Results are compared with experimental data showing good agreement. The general formulation can be employed for other smart materials.

After this introduction, Section 2 presents the mathematical formulation of the prismatic approach, using the Preisach model as a reference. Section 3 presents the SMA experimental investigation employed as a reference smart material case. Numerical simulations are then presented in Section 4, discussing temperature-dependent behavior, and Section 5, discussing cyclic-

dependent cases represented by transformation-induced plasticity. A numerical-experimental comparison is established showing good agreement. The conclusions are presented in Section 6.

## 2. Mathematical model

A novel triangular prism approach is proposed to describe the hysteretic behavior of smart materials. The novel model is based on the Preisach model, extending the classical triangular domain to create a prismatic domain that allows the description of distinct behaviors. Concerning SMAs, these behaviors include temperature-dependent behavior, transformation-induced plasticity, and classical plasticity. Initially, the Preisach domain is presented, and afterward, the novel model is discussed. The use of the Everett function is also presented.

### 2.1. Preisach model

The classic Preisach model offers a comprehensive framework capable of capturing various hysteretic phenomena. This model is built from mathematical operators defined within an abstract space, referred to as Preisach hysteresis operators, which correspond to two states. The Preisach operator,  $\hat{\gamma}_{\alpha\beta}$ , is represented by rectangular loops in an input-output diagram to illustrate hysteretic behavior (Mayergoyz, 1991). Furthermore, this operator is associated with abstract variables  $\alpha$  and  $\beta$ , which correspond to two directions of transformation. Figure 1 shows the operator as a function of an input, such as the strain ( $\varepsilon$ ) characterized by different paths for increasing ( $a-b-c-d-e$ ) or decreasing ( $e-d-f-b-a$ ) inputs.

A generic hysteresis can be represented as a series of elementary transformations, being expressed through the superposition of operations defined by hysteresis operators. On this basis, the classical Preisach

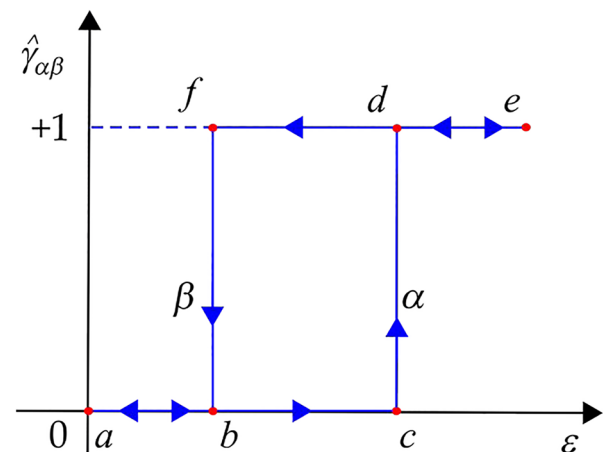


**Figure 1.** Definition of the Preisach hysteresis operator associated with abstract variables  $\alpha$  and  $\beta$ , which correspond to two directions of transformation.

formulation is established defining an output (stress) as a function of the input (strain) expressed as follows:

$$\tilde{\sigma}(\varepsilon) = \hat{\Gamma}\varepsilon \equiv \int_{\alpha_0}^{\alpha_n} \int_{\beta_0}^{\beta_n} \mu(\alpha, \beta) \hat{\gamma}_{\alpha\beta} d\alpha d\beta, \quad (1)$$

where  $\mu(\alpha, \beta)$  denotes the Preisach function, and  $\hat{\Gamma}$  represents the Preisach hysteresis operator. Furthermore,  $\alpha_0$  and  $\beta_0$  represent the smallest values while  $\alpha_n$  and  $\beta_n$  represent the highest values.

The geometric interpretation of the Preisach approach is illustrated in Figure 2. Figure 2(a) presents the input evolution showing the prescribed strain, divided into four loading-unloading cycles, associated with 12 points, 1–12. Figure 2(b) shows the stress-strain curve, representing the four loading cycles subdivided into seven regions through vertical lines. Figure 2(c) shows the Preisach triangle, illustrating the points corresponding to each stage of the loading process. The triangle is built considering that an increase in strain shifts the value along the  $\alpha$ -axis, while a decrease shifts it along the  $\beta$ -axis (Alvares et al., 2024).

The correlation of the stress-strain curve and the Preisach domain is better explained by considering Figure 3. The first point (1) is represented in the lower part of the triangle on the left. The loading process causes a vertical shift through variable  $\alpha$  that fills the triangular domain reaching the highest strain value (point 4), represented by green color. The subsequent unloading process is represented by a horizontal shift from point 4 to point 7, starting at the line defined by  $\alpha = \beta$ . Once again, the green color establishes the shift. The second loading cycle begins at point 7, which should be a vertical shift that finishes at point 10. At point 10, the second unloading cycle starts, being associated with another horizontal shift. These four cycles together establish the construction of the Preisach triangle showed in Figures 2(c) and 3.

## 2.2. Everett function

Mayergoz (1991) reformulated the classical Preisach approach by replacing the integration with a summation, or in other words, the Preisach function by the Everett function ( $F$ ) (Khan and Lagoudas, 2002). Therefore, equation (1) is rewritten as a summation of Everett functions based on  $n$  loading steps:

$$\tilde{\sigma}(\varepsilon) \equiv \sum_{k=1}^n [F(\alpha_k, \beta_{k-1}) - F(\alpha_k, \beta_k)]. \quad (2)$$

The Everett function is associated with a surface related to the Preisach triangular domain, defining the coordinate points  $(\alpha, \beta, F)$ . Therefore, the hysteretic behavior is described from the Everett surface, which is built from experimental data. The coordinate  $F$  is obtained through the stress matrix  $H_{\alpha\beta}$ , where  $\alpha$  represents the columns while  $\beta$  represents rows. On this basis, the loading is represented by the variation of  $\alpha$ , changing columns in the same row. On the other hand, the unloading is represented by the variation of  $\beta$ , changing rows in the same column (constant  $\alpha$ ). The calculation of the  $F$  coordinate is performed considering a formation rule for each row and column, as summarized in Table 1 (Alvares et al., 2024). The values of the first row ( $\beta_0$ ) represent the loading between points 1–4 (first loading cycle) being obtained by subtracting the lowest stress value ( $\sigma_1$ ) from the stress values of each experimental point within this cycle. On the other hand, the values in column eight ( $\alpha_7$ ) represent loading cycle 4–7 (first unloading cycle), being calculated by subtracting the highest stress value ( $\sigma_4$ ) from the stress values of each experimental point within this cycle. Similarly, for the second loading cycle, represented by points 7–10, is described in row two ( $\beta_1$ ), subtracting the lowest stress value ( $\sigma_7$ ) from the stress values of each experimental point within this cycle. Finally, the unloading represented by points 10–12 is described in column seven ( $\alpha_6$ ) following the same idea. On this

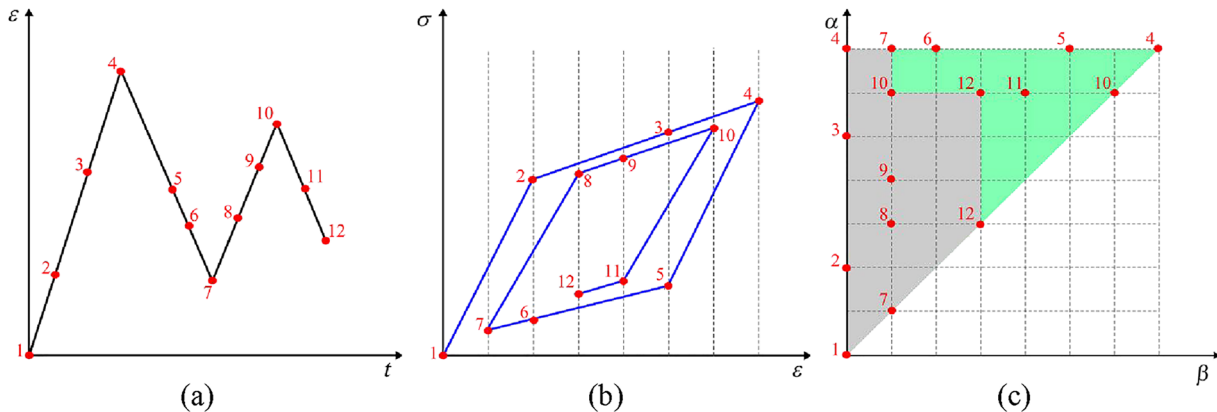


**Figure 2.** Preisach triangle mapping: (a) loading-unloading history, (b) stress-strain from seven divisions of the hysteresis region, and (c) Preisach triangle obtained from the proposed division.

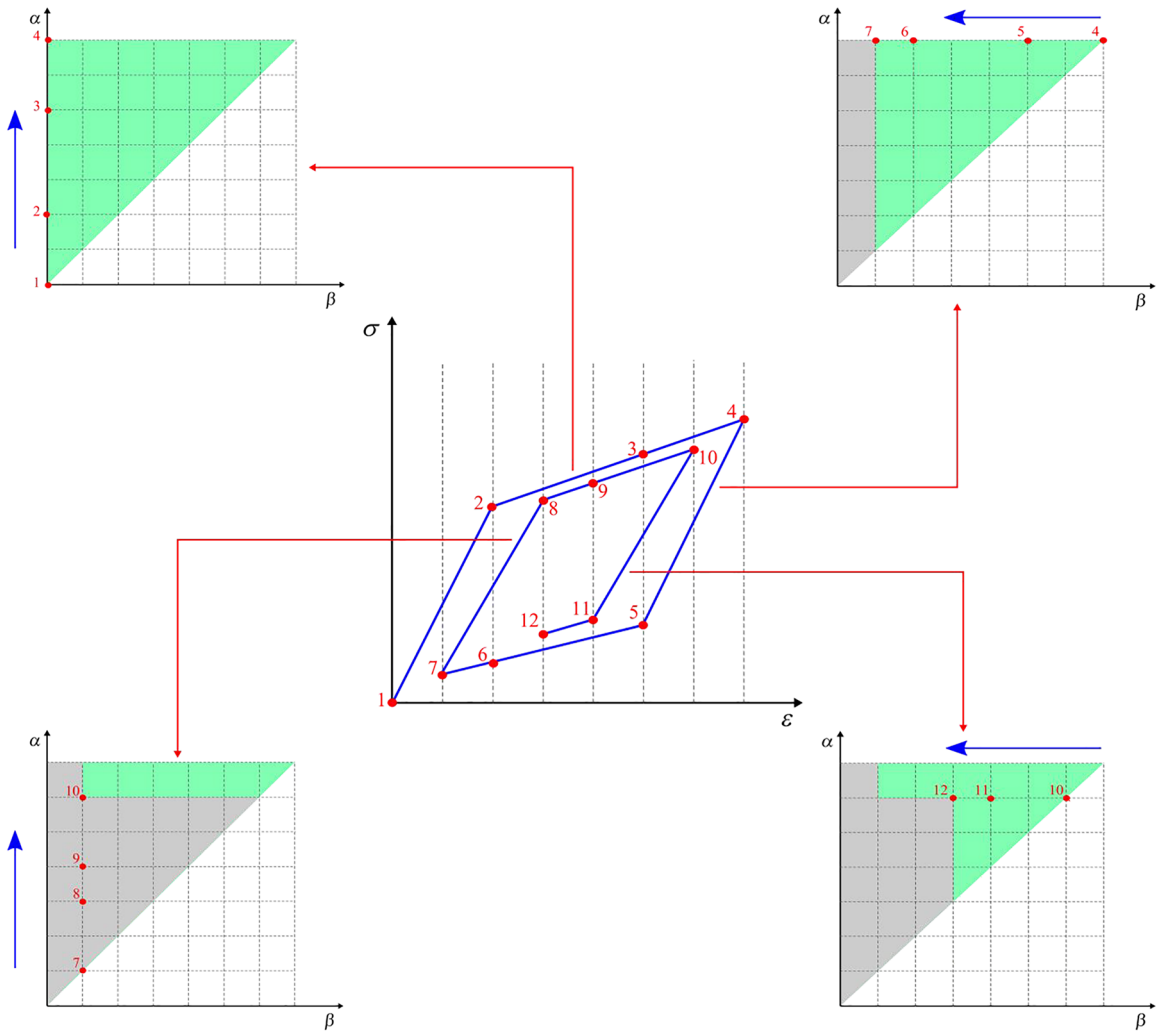


**Figure 3.** Construction of the Preisach triangle considering each stage of the loading-unloading process.

**Table 1.** Determination of the  $H_{\alpha\beta}$  matrix associated with the Everett function.

	$\alpha_0$	$\alpha_1$	$\alpha_2$	$\alpha_3$	$\alpha_4$	$\alpha_5$	$\alpha_6$	$\alpha_7$
$\beta_0$	$\sigma_1 - \sigma_1$	0	$\sigma_2 - \sigma_1$	0	0	$\sigma_3 - \sigma_1$	0	$\sigma_4 - \sigma_1$
$\beta_1$	0	$\sigma_7 - \sigma_7$	0	$\sigma_8 - \sigma_7$	$\sigma_9 - \sigma_7$	0	$\sigma_{10} - \sigma_7$	$\sigma_4 - \sigma_7$
$\beta_2$	0	0	0	0	0	0	0	$\sigma_4 - \sigma_6$
$\beta_3$	0	0	0	0	0	0	$\sigma_{10} - \sigma_{12}$	0
$\beta_4$	0	0	0	0	0	0	$\sigma_{10} - \sigma_{11}$	0
$\beta_5$	0	0	0	0	0	0	0	$\sigma_4 - \sigma_5$
$\beta_6$	0	0	0	0	0	0	$\sigma_{10} - \sigma_{10}$	0
$\beta_7$	0	0	0	0	0	0	0	$\sigma_4 - \sigma_4$

basis, the main diagonal is always null since it is the initial value of the cycle minus the first value. The Everett surface is presented in Figure 4 highlighting the points illustrated in the previous Figures 2 and 3.

### 2.3. Prismatic approach

The *triangular Preisach domain* can be extended to incorporate an extra variable to represent distinct

effects. In this regard, a *prismatic domain* is defined considering a third coordinate to represent different phenomena associated with smart materials. On this basis, a prismatic approach is proposed using a *triangular prism domain*.

To illustrate the construction of the prismatic domain, it is considered that the material behavior varies according to the evolution of some variable that defines an extra dimension. It is assumed stress-strain

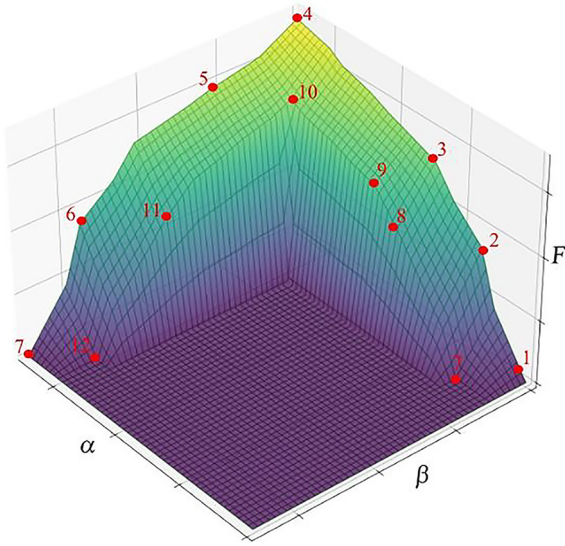


**Figure 4.** Everett surface associated with the loading-unloading process.

curves that can vary according to an extra variable  $\xi$ . Using SMA thermomechanical behavior as a reference, either temperature-dependent or cyclic-dependent behaviors are examples of these phenomena represented by the extra variable. By considering two different values of this variable,  $\xi_1$  and  $\xi_2$ , experimental stress-strain curves are built for each one of these values, Figure 5. On this basis, each one of them can be treated by the Preisach triangle and the respective Everett surface. Since two different domains are defined, a prismatic interpolation can be performed to evaluate the stress-strain curve in any intermediate  $\xi$ -value,  $\xi_i$ . Figure 5 schematically shows the procedure for constructing the novel prismatic domain, representing the  $\xi$ -value based on experimental results. This procedure allows the description of any intermediate  $\xi$ -value based on reference values. In other words, the prismatic domain is built assuming a third dimension connecting different triangular Preisach domains, and this dimension can represent different kinds of variables, allowing it to represent different phenomena.

The prismatic approach employs the triangular domain represented by variables  $\alpha$  and  $\beta$ , together with a new variable,  $\xi$ , that represents different phenomena. Therefore, a new integration can be defined through this new variable,

$$\begin{aligned} \sigma(\varepsilon, \xi) &= \Xi(\tilde{\sigma}) = \Xi(\hat{\Gamma}\varepsilon) \equiv \int_{\xi_0}^{\xi_n} \tilde{\sigma} d\xi \\ &= \int_{\xi_0}^{\xi_n} \left[ \int_{\alpha_0}^{\alpha_n} \int_{\beta_0}^{\beta_n} \mu(\alpha, \beta) \hat{\gamma}_{\alpha\beta} d\alpha d\beta \right] d\xi, \end{aligned} \quad (3)$$

where  $\xi_0$  and  $\xi_n$  represent, respectively, the smallest and largest values of  $\xi$ .

The Everett function can be defined in a similar way by establishing a proper interpolation, represented by  $\Theta$ , between two different surfaces defined for each  $\xi$ -value,

$$\sigma(\varepsilon, \xi) \equiv \Theta(F_1, F_2), \quad (4)$$

where each triangular domain  $j$  is defined from the general definition,

$$F_j = \sum_{k=1}^n F(\alpha_k, \beta_{k-1}, \xi_j) - F(\alpha_k, \beta_k, \xi_j). \quad (5)$$

Essentially, these new operations can be interpolated from the classical Preisach approximations. Different interpolation approaches can be employed, and linear interpolation showed to be appropriate for most of the cases. The situations where the linear interpolation does not present good approximation can be overcome by considering a better discretization, increasing the number of necessary triangular domains.

The computational effort related to the Prismatic approach is considerable less than the usual algorithms employed to deal with nonlinear thermodynamic-based constitutive models, being related to the construction of matrix  $H_{\alpha\beta}$  and the interpolation process.

### 3. SMA experimental investigation

Shape memory alloys are selected to evaluate the general hysteretic behavior of smart materials. Experimental tests are developed in order to evaluate the temperature-dependent behavior and cyclic-dependent pseudoelastic behavior associated with transformation-induced plasticity.

Temperature-dependent behavior defines the shape memory effect for low-temperature behavior and pseudoelasticity for high-temperature behavior. These behaviors are essentially defined by the phase transformations that can be induced either by stress or temperature. The critical phase transformation stress values are temperature-dependent which promotes a shift of the hysteresis loop, characterizing both behaviors.

On the other hand, transformation-induced plasticity (TRIP) is a typical example of cyclic-dependent behavior, which is defined as the plastic flow arising from solid-state phase transformation processes involving volume and/or shape changes without overlapping the yield surface. This phenomenon occurs in shape memory alloys having significant influence over their macroscopic thermomechanical behavior. The main characteristic observed in the stress-strain curves during the cyclic loading process is the reduction of the phase transformation stress and the increase of the residual permanent strain, which characterizes the TRIP effect.

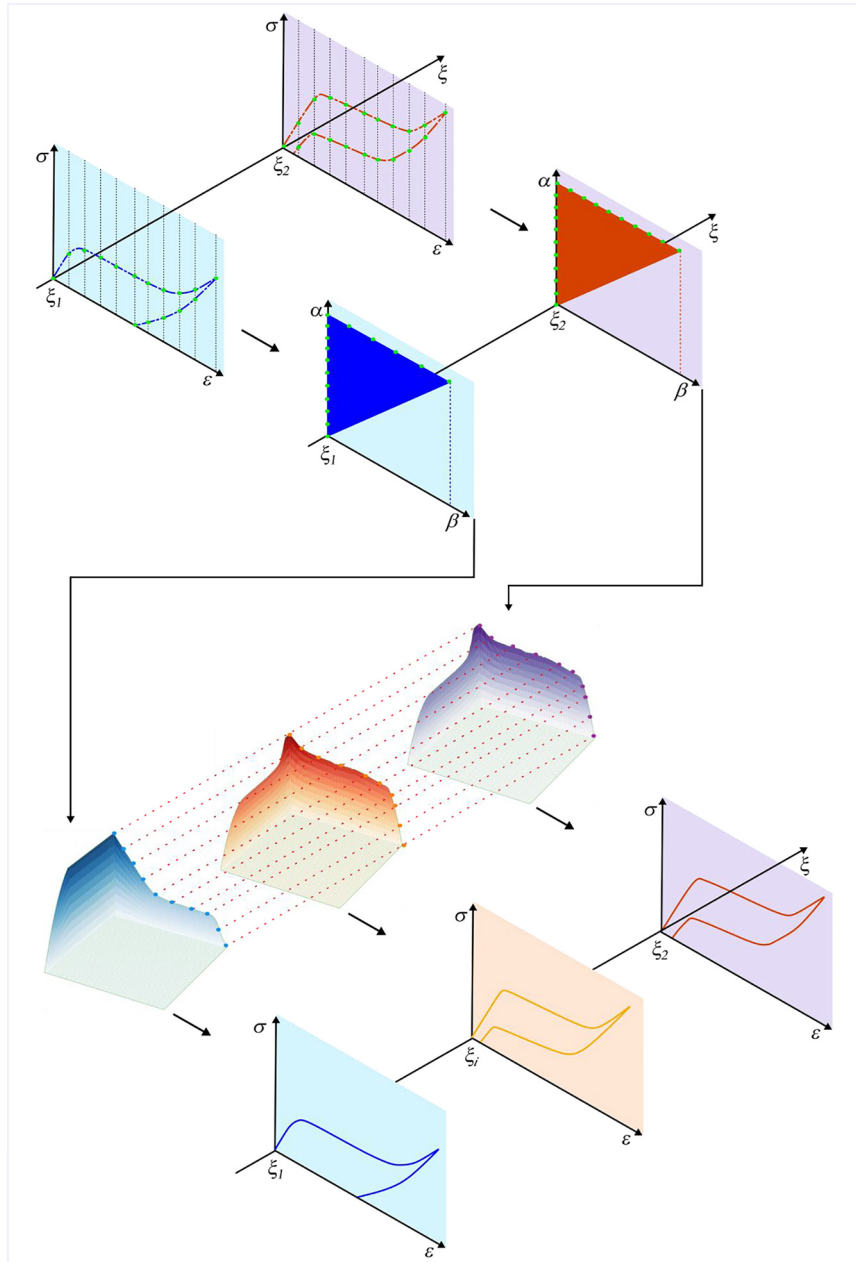


**Figure 5.** Prismatic approach: triangular prism domain is built introducing an extra variable  $\xi$  to the classical Preisach triangle ( $\alpha, \beta$ ). Two different experimental tests are built and each one of them is related to the Preisach model, with a triangular domain ( $\alpha, \beta$ ), and an Everett function. An interpolation is then performed through these values, allowing the description of the third dimension,  $\xi$ .

This feature establishes a training process in order to stabilize stress-strain curves before the use of SMA for applications.

SMA samples are employed for this aim using Ni56Ti44 circular section wire in an as-received condition, with a diameter of 1.30 mm (Sandinox biomaterials). Thermomechanical tests are performed considering a differential scanning calorimeter (DSC), NETZSCH Maia 200 F3, and tensile tests using an electro-mechanical testing machine, Instron 5882, employing a 30 kN static load cell and strain

measurement based on displacement with a gauge length of 100 mm.

The phase transformation temperatures are measured from DSC tests using a virgin wire sample. During the test, the sample is heated from room temperature to 393 K and then cooled to 153 K. After that, this cycle is repeated. Figure 6 shows the results of this test, highlighting the transformation temperatures of the start and finish of austenitic formation ( $A_s, A_f$ ) and the start and finish of martensitic formation ( $M_s, M_f$ ). During heating, there are two regions of phase

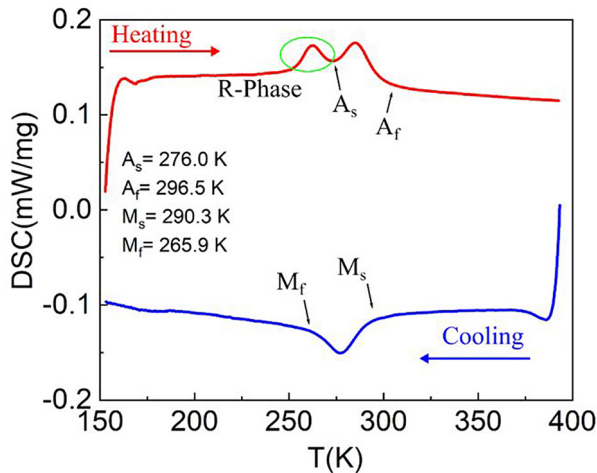


**Figure 6.** DSC thermal analysis of a virgin NiTi wire allowing the determination of the phase transformation temperature. The sample is heated from room temperature to 393 K and then cooled to 153 K. After that, this cycle is repeated.

transformation (martensite  $\rightarrow$  R-phase and R-phase  $\rightarrow$  austenite) and a peak of transformation during cooling (austenite  $\rightarrow$  martensite). In this regard, for temperatures above  $A_f$  (296.5 K) austenitic phase is stable and the SMA presents a pseudoelastic behavior when subjected to mechanical loading. On the other hand, for temperatures below  $M_f$  (265.9 K) martensite phase is stable and the SMA presents the shape memory effect.

After the DSC test, a macroscopic verification is performed considering stress-strain curves at different temperatures. In this regard, the specimen is subjected to a quasi-static tensile test with a peak stress of 900 MPa and a stress rate of 150 MPa  $\text{min}^{-1}$ . Six tests are carried out considering different temperatures: 258, 292, 298, 303, 313, and 318 K. For each test, a new sample of virgin wire is used presenting non-stabilized results as showed in Figure 7. Therefore, it is noticeable that TRIP is evolving during the tests, which is characterized by a residual strain after the unloading. This means that these results are contemplating both temperature-dependent and cyclic-dependent data. Note that at the temperature of 258 K (below  $M_f$ ), the material presents the shape memory effect. On the other hand, for the other temperatures, the material is characterized by pseudoelastic behavior with the presence of a residual strain due to TRIP after the mechanical load removal. Furthermore, throughout the tests, the temperature increase is associated with a hysteresis shift, which is related to an increase of phase transformation critical stresses (stresses where the start and finish of phase transformations occur).

The SMA cyclic-dependent response is evaluated by considering a specimen subjected to a training process considering a quasi-static cyclic tensile test with a peak stress of 900 MPa and a stress rate of 150 MPa  $\text{min}^{-1}$ . SMA training can be conducted by applying cyclic

mechanical loading until a stabilized response is reached. This stabilization process represents the effect of the TRIP strain, being an essential procedure for the use of shape memory alloys, enabling repeatability. Figure 8(a) shows the stress-strain curves obtained from 25 cycles. Note the stabilization of the TRIP strain throughout the cycles, the decrease in the size of the hysteresis loop, and the reduction of the phase transformation critical stresses, where the phase transformations start and finish. Figure 8(b) presents the evolution of the strain experienced by the sample over the cycles, indicating a stabilization after approximately 20 cycles.

Numerical simulations are carried out in the sequel to evaluate the model capabilities to describe the thermomechanical behaviors of SMAs. It should be pointed out that experimental data has temperature-dependent and cyclic-dependent behaviors.

#### 4. Numerical simulations: Temperature-dependent behavior

The SMA temperature-dependent behavior is now of concern considering the experimental tests developed in the previous section as reference. The idea is to establish the model capability to describe the SMA thermo-mechanical behavior. Experimental tests at  $T = 258\text{K}$  (shape memory effect) and  $T = 318\text{K}$  (pseudoelasticity), presented in Figure 7, are employed to establish the Preisach triangles and Everett surfaces. On this basis, 100 divisions of the experimental stress-strain space are used to obtain the experimental points to build the Preisach triangle. Figure 9 shows the numerical-experimental comparison where it is possible to observe that the Preisach model can represent the shape memory effect and pseudoelasticity of shape memory alloys with good agreement. The Everett surfaces obtained for both temperatures are also presented. It should be pointed out that the simulations capture the phase transformation together with transformation-induced plasticity responsible for the residual strain of the high-temperature behavior.

Based on the results of the Preisach model, prismatic interpolation can be employed to evaluate any temperature contained in the interval between both curves described by the Preisach model. On this basis, temperature is the third dimension of the prisma and numerical-experimental comparisons are established for the following temperatures: 292, 298, 303, and 313 K. Figure 10 presents results for these intermediate temperatures, and results once again present a good agreement. It should be observed that experimental data presents transformation-induced plasticity, and the model is able to capture this behavior with good agreement. Therefore, the novel triangular prism approach is capable of capturing the general SMA

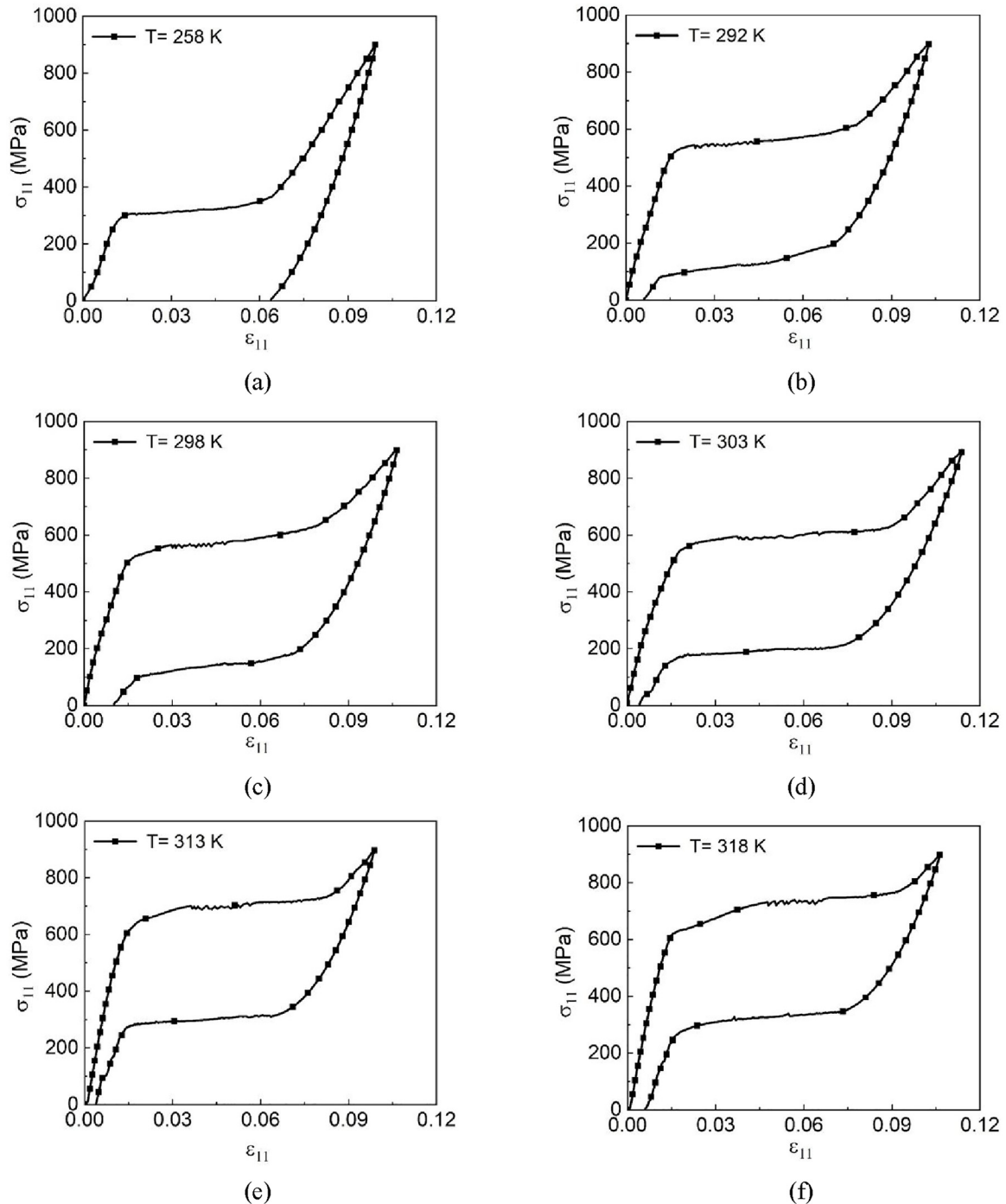


**Figure 7.** Tensile test of a NiTi wire in different temperatures with a peak stress of 900 MPa and a stress rate of  $150 \text{ MPa min}^{-1}$ : (a)  $T = 258 \text{ K}$ , (b)  $T = 292 \text{ K}$ , (c)  $T = 298 \text{ K}$ , (d)  $T = 303 \text{ K}$ , (e)  $T = 313 \text{ K}$ , and (f)  $T = 318 \text{ K}$ .

thermomechanical behavior from two reference temperatures, making the model a versatile tool for describing the temperature-dependent behavior of SMAs.

## 5. Numerical simulations: Cyclic-dependent behavior

The description of cyclic-dependent responses is now analyzed considering the proposed approach.

Transformation-induced plasticity (TRIP) is employed as a reference case, using the experimental tests of Figure 8. On the basis, the evolution of the TRIP strain along the cycles is adopted as the third coordinate for the building of the prismatic domain, using the first and last cycles of the experimental result to define the Preisach triangles and Everett surfaces. Once again, 100 divisions of the experimental stress-strain curve are used to build the Preisach triangle and Figure 11 shows

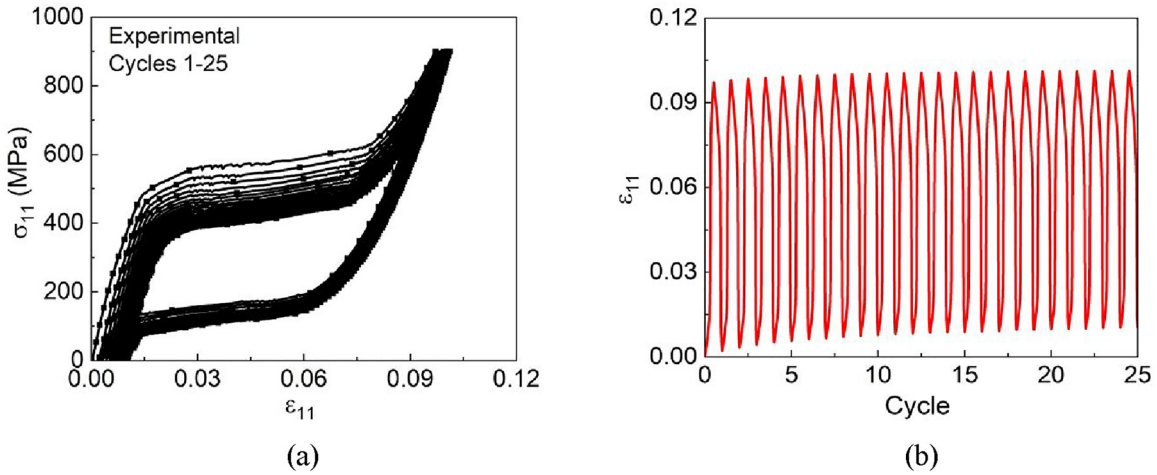


**Figure 8.** Quasi-static tensile tests of a pseudoelastic NiTi wire at a temperature of 303 K, training procedure at a maximum stress of 900 MPa, and a loading rate of 150 MPa min<sup>-1</sup>: (a) cyclic stress-strain response presenting 25 cycles, (b) TRIP strain stabilization throughout the cycles.

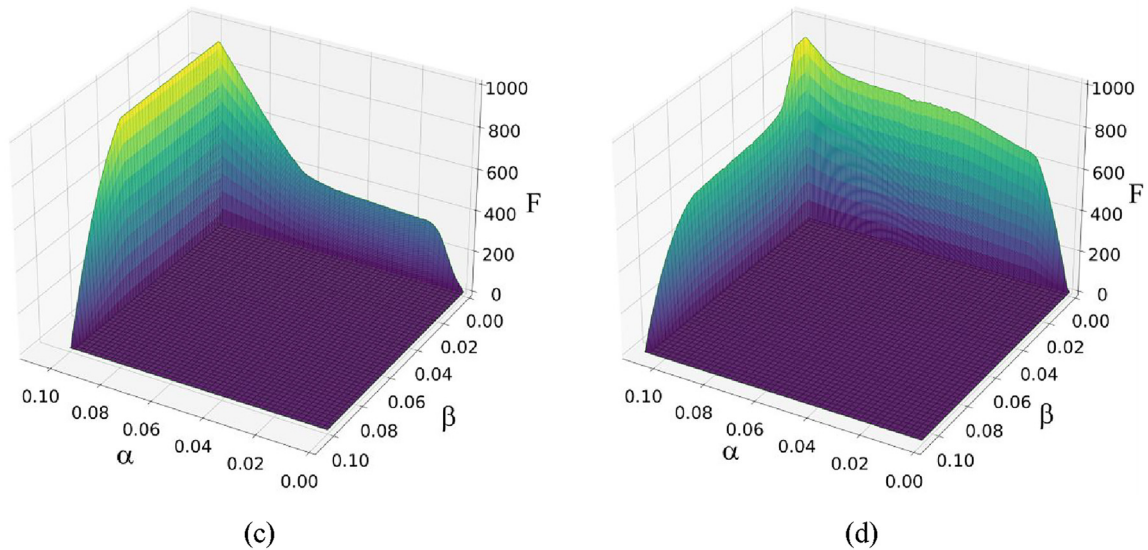
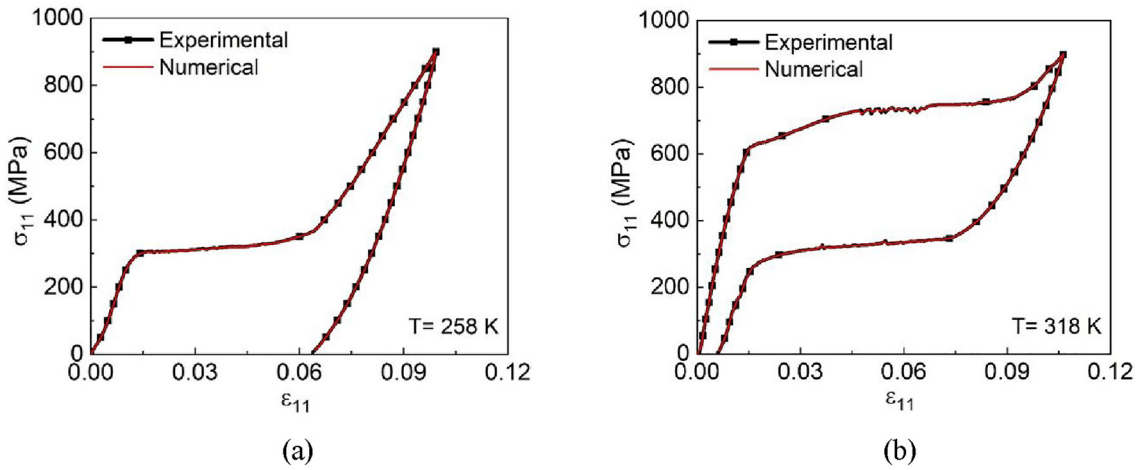


**Figure 9.** Preisach model employed to describe the stress-strain curves for two reference temperatures: (a) numerical-experimental comparison at 258 K, (b) numerical-experimental comparison at 318 K, (c) Everett surface at 258 K, and (d) Everett surface at 318 K.

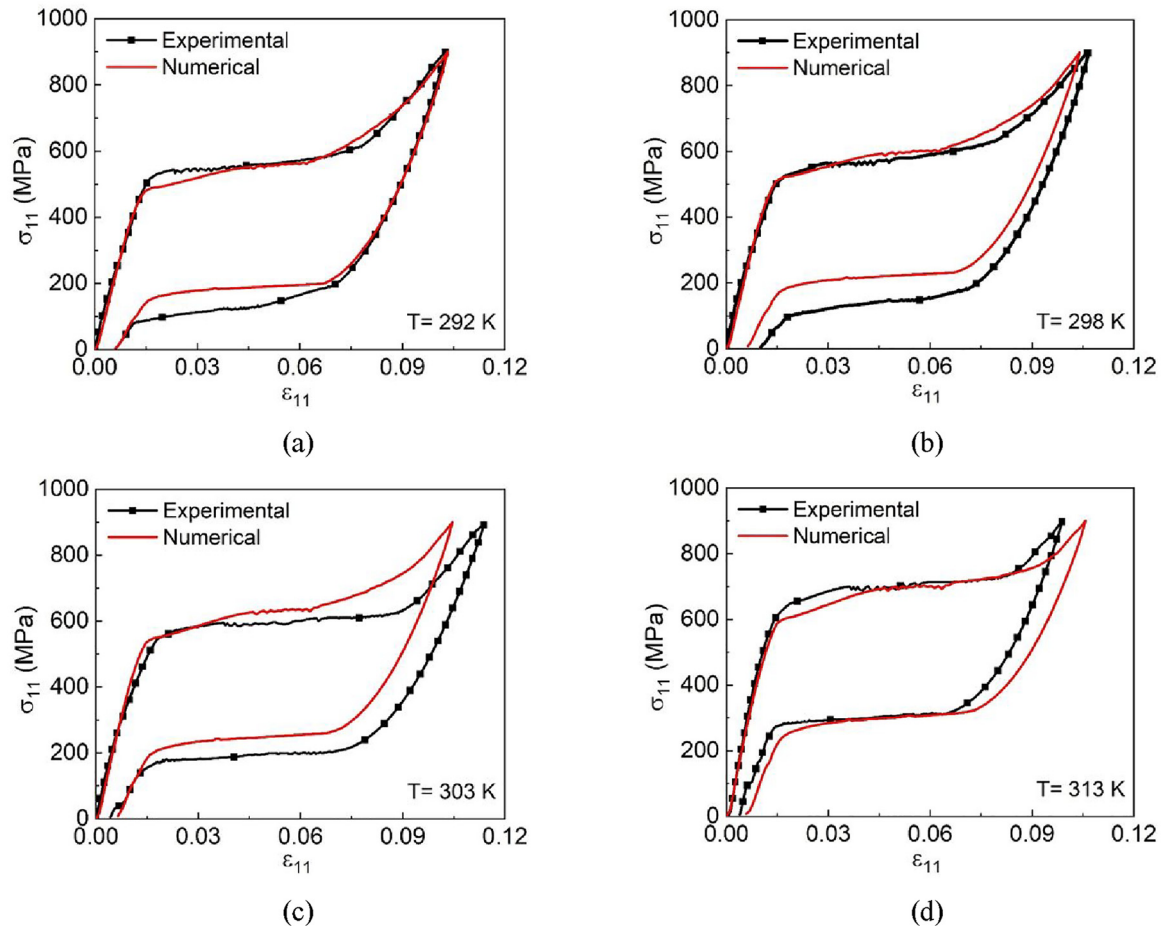


**Figure 10.** Stress-strain curves predicted by the model considering intermediate temperatures, together with experimental data: (a) 292 K, (b) 298 K, (c) 303 K, and (d) 313 K.

the numerical-experimental comparison for the reference cases together with the Everett surfaces. A good agreement is observed, showing the ability of the Preisach model to match the pseudoelastic response.

The prismatic approach is now of concern in order to represent intermediate cycles during TRIP strain evolution. Figure 12 shows a numerical-experimental comparison considering intermediate cycles: 2, 6, 10, 15, 20, and 24. Once again, it should be pointed out the good agreement between numerical and experimental results, showing the prismatic model capability to describe the general SMA pseudoelastic response, including the stabilization process of the TRIP strain.

## 6. Conclusions

This work proposes a novel prismatic approach, based on the Preisach model, to describe hysteretic behavior of smart materials. The classical Preisach model is defined from elementary operators defined within an abstract triangular space. The novel model adopts a prismatic domain that extends the triangular domain

incorporating a new axis that can represent variables associated with distinct phenomena.

Shape memory alloy thermomechanical behavior is adopted as a case study, being representative of other smart materials. Thermal and mechanical experimental tests of NiTi wires are employed to establish reference cases. Mechanical tests consider temperature-dependent behavior including shape memory effect and pseudoelasticity. In addition, cyclic loading tests are performed to observe transformation-induced plasticity, showing typical SMA training tests.

Based on the reference experimental data, the Preisach model is employed to match two cases related to either the temperature-dependent behavior or the TRIP phenomenon. Afterward, a prismatic approach is employed to evaluate intermediate situations, not adjusted by the original model. Concerning temperature-dependent behavior, shape memory and pseudoelastic cases are adjusted and afterward, intermediate temperatures are interpolated. Regarding the TRIP behavior, the first and last cycles are adjusted by the Preisach model, and afterward, intermediate cycles are interpolated from the prismatic approach.

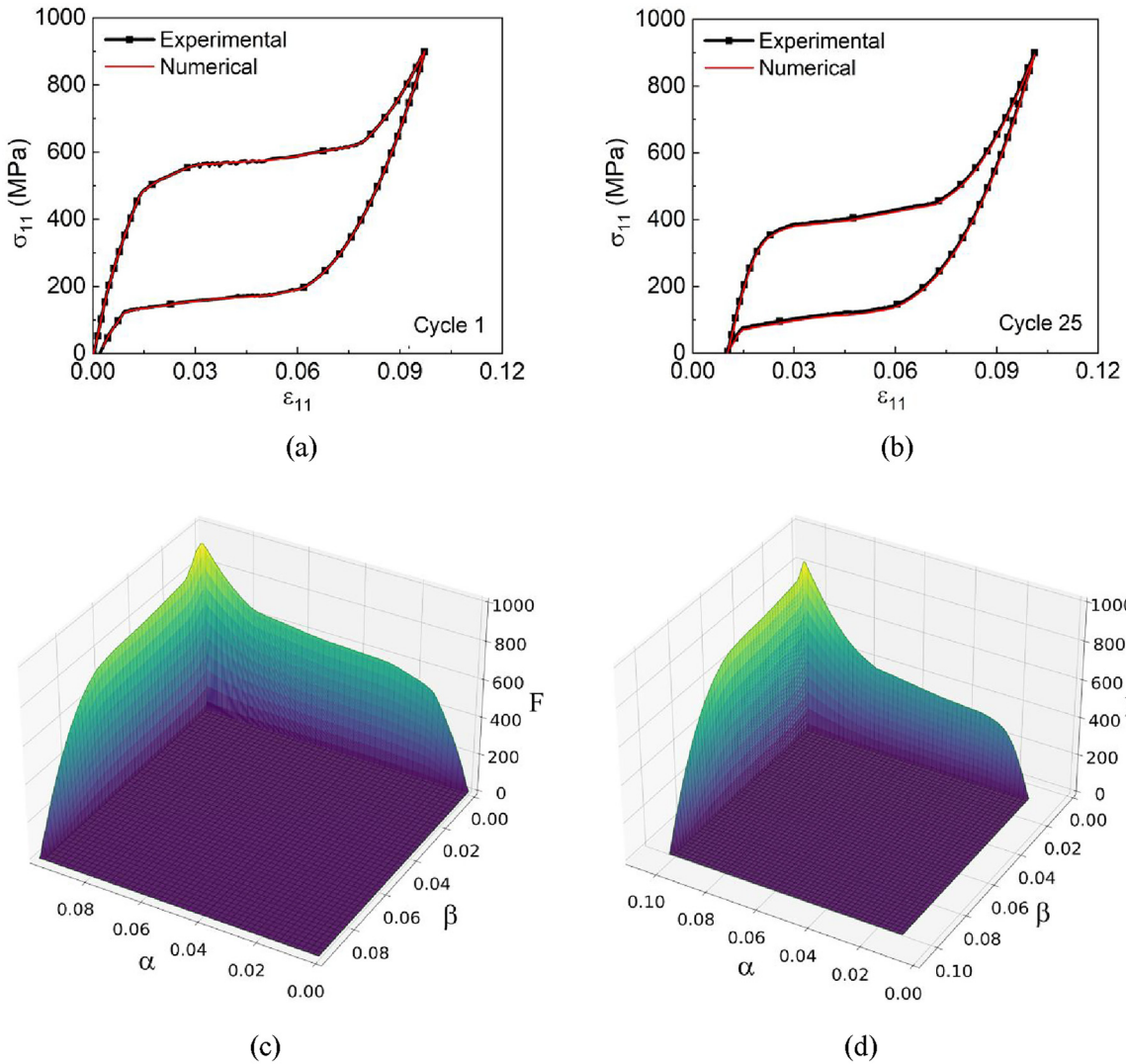


**Figure 11.** Preisach model employed to describe the stress-strain curves for two reference cycles related to transformation-induced plasticity tests: (a) numerical-experimental comparison at the first cycle, (b) numerical-experimental comparison at the last cycle, (c) Everett surface at the first cycle, and (d) Everett surface at the last cycle.

Numerical simulations are compared with experimental data showing very good agreements, attesting to the model capability to capture the main features of the hysteretic behavior of smart materials, particularly the SMA thermomechanical behavior, properly describing different aspects related to SMA behavior. The authors believe that this is a powerful data-driven approach in

which simplicity can be useful for several simulation purposes. Other smart materials can be analyzed with the same approach, showing the multidisciplinary characteristic of the model. In addition, it is possible to expand this approach considering hypersurfaces that include more than one extra axis, simultaneously treating different phenomena.

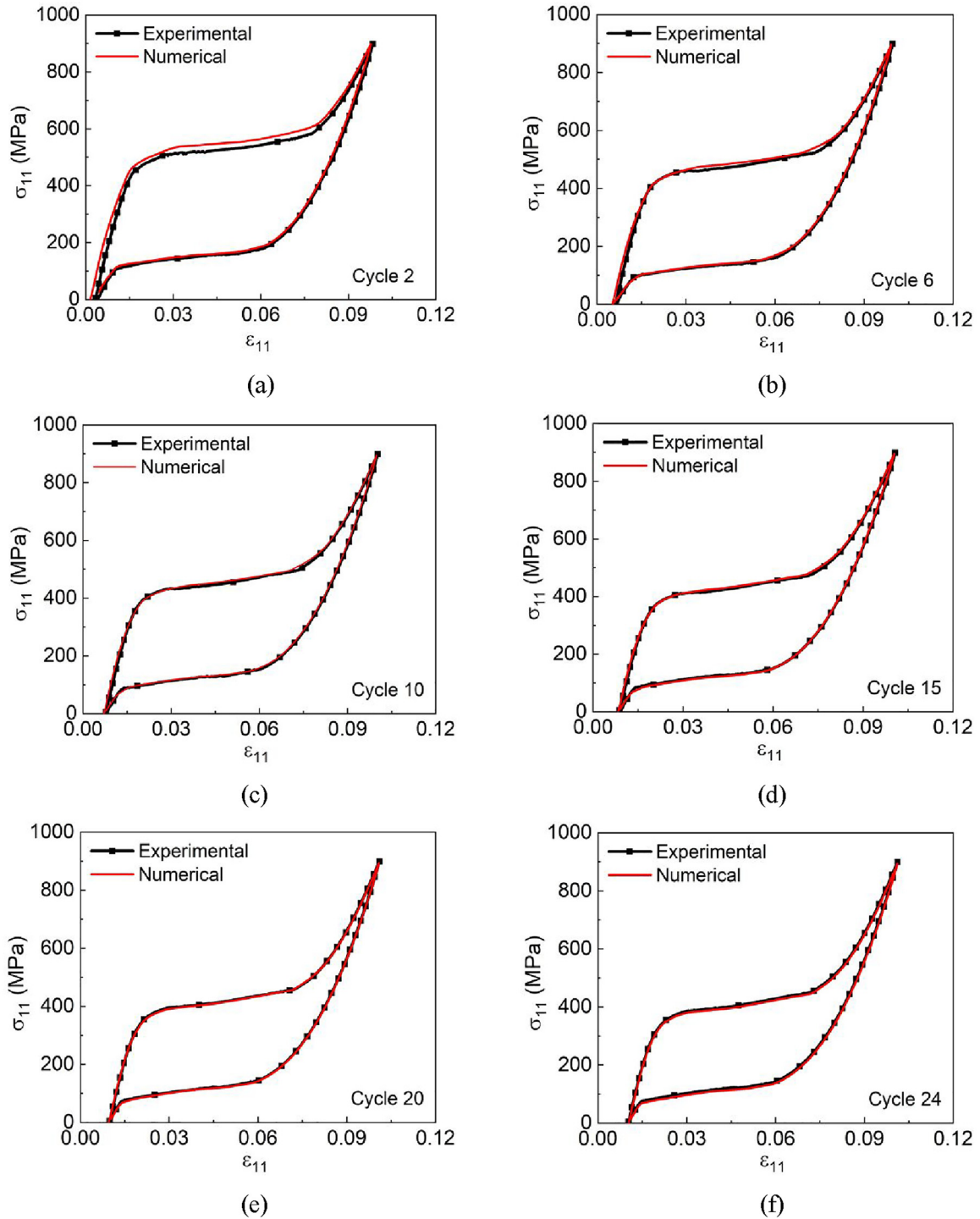


**Figure 12.** Stress-strain curves predicted by the model considering different cycles of the TRIP test, together with experimental data: (a) cycle 2, (b) cycle 6, (c) cycle 10, (d) cycle 15, (e) cycle 20, and (f) cycle 24.

## Declaration of conflicting interests

The authors declared no potential conflicts of interest with respect to the research, authorship, and/or publication of this article.

## Funding

The authors disclosed receipt of the following financial support for the research, authorship, and/or publication of this article: The authors would like to acknowledge the support of the Brazilian Research Agencies CNPq (Conselho Nacional de Desenvolvimento Científico e Tecnológico), CAPES (Coordenação de Aperfeiçoamento de Pessoal de Nível Superior), and FAPERJ (Fundação Carlos Chagas Filho de Amparo à Pesquisa do Estado do Rio de Janeiro) and through the INCT-EIE (National Institute of Science and Technology - Smart Structures in Engineering), and FAPEMIG (Fundação de Amparo à Pesquisa do Estado de Minas Gerais). The support of the AFOSR (Air Force Office of Scientific Research; FA9550-23-4301-0527) is also acknowledged.

## ORCID iD

Marcelo A. Savi  <https://orcid.org/0000-0001-5454-5995>

## Data availability

The datasets generated during and/or analyzed during the current study are available from the corresponding author upon reasonable request.

## References

- Adeodato A, Vignoli LL, Paiva A, et al. (2022) A shape memory alloy constitutive model with polynomial phase transformation kinetics. *Shape Memory and Superelasticity* 8: 277–318.
- Alsawalhi MY and Landis CM (2022) A new phenomenological constitutive model for shape memory alloys. *International Journal of Solids and Structures* 257: 111264.
- Alvares TQ, Dornelas VM, Oliveira SA, et al. (2024) Thermo-mechanical description of shape memory alloys using the Preisach model. *Smart Materials and Structures* 33: 1–19.
- Anumodh R, Singh B and Zuber M (2021) Morphing applications in automobiles: A review. *International Journal of Vehicle Design* 85(1): 1–31.
- Chang WS and Araki Y (2016) Use of shape-memory alloys in construction: A critical interview. *Proceedings of the Institution of Civil Engineers - Civil Engineering* 169(2): 87–95.
- Chaudhary K, Haribhakta VK and Jadhav PV (2024) A review of shape memory alloys in MEMS devices and biomedical applications. *Materials Today Proceedings*. 1–6.
- Chen Y, Shen X, Li J, et al. (2019) Nonlinear hysteresis identification and compensation based on the discrete Preisach model of an aircraft morphing wing device manipulated by an SMA actuator. *Chinese Journal of Aeronautics* 32, 4: 1040–1050.
- Chowdhury P (2018) Frontiers of theoretical research on shape memory alloys: A general overview. *Shape Memory and Superelasticity* 4(1): 26–40.
- Cisse C, Zaki W and Ben Zineb T (2016a) A review of constitutive models and modeling techniques for shape memory alloys. *International Journal of Plasticity* 76: 244–284.
- Cisse C, Zaki W and Zineb TB (2016b) A review of modeling techniques for advanced effects in shape memory alloy behavior. *Smart Materials and Structures* 25: 103001.
- Davino D, Natale C, Pirozzi S, et al. (2004) Phenomenological dynamic model of a magnetostrictive actuator. *Physica B Condensed Matter* 343(1–4): 112–116.
- Dong Y, Hu H and Wang H (2014) Identification and experimental assessment of two-input Preisach model for coupling hysteresis in piezoelectric stack actuators. *Sensors and Actuators A Physical* 220: 92–100.
- Doraiswamy S, Rao A and Srinivasa AR (2011) Combining thermodynamic principles with Preisach models for super-elastic shape memory alloy wires. *Smart Materials and Structures* 20(8): 085032.
- Dornelas VM, Oliveira SA and Savi MA (2020) A macroscopic description of shape memory alloy functional fatigue. *International Journal of Mechanical Sciences* 170: 105345.
- Dornelas VM, Oliveira SA, Savi MA, et al. (2021) Fatigue on shape memory alloys: Experimental observations and constitutive modeling. *International Journal of Solids and Structures* 213: 1–24.
- Elahinia MH (2016) *Shape Memory Alloy Actuators: Design, Fabrication, and Experimental Evaluation*. New York, NY: John Wiley & Sons Ltd.
- Fonseca LM, Rodrigues GV and Savi MA (2022) An overview of the mechanical description of origami-inspired systems and structures. *International Journal of Mechanical Sciences* 223: 107316.
- Gao X, Feng Z, Zhu H, et al. (2024) Modeling and simulation of magnetostrictive actuators based on  $\Delta E$  effect Preisach model. *Journal of Physics: Conference Series IOP Publishing* 2741, 1: 012046.
- Gorbet RB, Wang DW and Morris KA (1998) Preisach model identification of a two-wire SMA actuator. In: *Proceedings. 1998 IEEE International Conference on Robotics and Automation*, Leuven, Belgium, vol. 3, pp. 2161–2167. IEEE.
- Hasan MM and Baxevanis T (2022) Structural fatigue and fracture of shape memory alloy actuators: Current status and perspectives. *Journal of Intelligent Material Systems and Structures* 33(12): 1475–1486.
- Hasan MM, Zhang M and Baxevanis T (2022) A finite-strain phase-field description of thermomechanically induced fracture in shape memory alloys. *Shape Memory and Superelasticity* 8(4): 356–372.
- He B, Dong X, Nie R, et al. (2023) Comprehensive shape memory alloys constitutive models for engineering application. *Materials & Design* 225: 111563.
- Hossain MS, Iyer R, Clemente CS, et al. (2023) Parameter identification for a model for multi-functional materials with hysteresis and thermodynamic compatibility. *Journal of Intelligent Material Systems and Structures* 34(19): 2280–2292.
- Hughes D and Wen JT (1997) Preisach modeling of piezoceramic and shape memory alloy hysteresis. *Smart Materials and Structures* 6(3): 287–300.
- Hughes DC and Wen JT (1995) Preisach modeling and compensation for smart material hysteresis. In: *Active materials and smart structures*, vol. 2427, pp.50–64. SPIE.

- Isgalgue A, Lovey FC, Terriault P, et al. (2006) SMA for dampers in civil engineering. *Materials Transactions* 47: 682–690.
- Janke L, Czaderski C, Motavalli M, et al. (2005) Applications of shape memory alloys in civil engineering structures - overview, limits and new ideas. *Materials and Structures* 38: 578–592.
- Kan Q, Zhang Y, Xu Y, et al. (2023) Tension-compression asymmetric functional degeneration of super-elastic NiTi shape memory alloy: Experimental observation and multi-scale constitutive model. *International Journal of Solids and Structures* 280: 112384.
- Karakalas AA, Machairas TT, Solomou AG, et al. (2019) Modeling of partial transformation cycles of SMAs with a modified hardening function. *Smart Materials and Structures* 28(3): 035014.
- Khandelwal A and Buravalla V (2009) Models for shape memory alloy behavior: An overview of modeling approaches. *The International Journal of Structural Changes in Solids* 1(1): 111–148.
- Khan MM and Lagoudas DC (2002) Modeling of shape memory alloy pseudoelastic spring elements using Preisach model for passive vibration isolation In: *Smart structures and materials 2002: Modeling, signal processing, and control*, vol. 4693, pp.336–347.
- Kumar EK, Patel SS, Panda SK, et al. (2024) A comprehensive exploration of shape memory alloys: Fundamentals, structural reinforcements, nano-analysis, machine learning perspective, and emerging applications. *Mechanics of Advanced Materials and Structures* 31: 11450–11534.
- Labusch M, Schröder J and Lupascu DC (2019) 3D magnetostrictive Preisach model for the analysis of magneto-electric composites. *Archive of Applied Mechanics* 89: 1011–1030.
- Lagoudas DC (2008) *Shape Memory Alloys, Modeling and Engineering Applications*. Austin, TX: Springer.
- Leal PB, Savi MA and Hartl DJ (2018) Aero-structural optimization of shape memory alloy-based wing morphing via a class/shape transformation approach. *Proceedings of the Institution of Mechanical Engineers Part G Journal of Aerospace Engineering* 232(15): 2745–2759.
- Leal PBC and Savi MA (2018) Shape memory alloy-based mechanism for aeronautical application: Theory, optimization and experiment. *Aerospace Science and Technology* 76: 155–163.
- Lecce L and Concilio A (2015) *Shape Memory Alloy Engineering for Aerospace, Structural and Biomedical Applications*. Oxford: Butterworth-Heinemann.
- Leo DJ (2007) *Engineering Analysis of Smart Material Systems*. Hoboken, NJ: John Wiley and Sons.
- Liu R, Zhang C, Ji H, et al. (2023) Training, control and application of SMA-Based actuators with two-way shape memory effect. *Actuators* 12(1): 1–25.
- Li Z, Su CY and Chai T (2013) Compensation of hysteresis nonlinearity in magnetostrictive actuators with inverse multiplicative structure for Preisach model. *IEEE Transactions on Automation Science and Engineering* 11(2): 613–619.
- Machado LG and Savi MA (2003) Medical applications of shape memory alloys. *Asian Journal of Medical and Biological Research* 36(6): 683–691.
- Mayergoz ID (1991) *Mathematical Models of Hysteresis*. New York, NY: Springer Verlag.
- Mayergoz ID (2003) *Mathematical Models of Hysteresis and Their Applications*. College Park, MD: Academic Press.
- Mohd Jani J, Leary M, Subic A, et al. (2013) A review of shape memory alloy research, applications and opportunities. *Materials & Design* 56: 1078–1113.
- Nair VS and Nachimuthu R (2022) The role of NiTi shape memory alloys in quality of life improvement through medical advancements: A comprehensive review. *Proceedings of the Institution of Mechanical Engineers* 236(7): 923–950.
- Nematollahi M, Baghbaderani KS, Amerinatanzi A, et al. (2019) Application of NiTi in assistive and rehabilitation devices: A review. *Bioengineering* 6(2): 37.
- Oliveira SA, Savi MA and Zouain N (2016) A three dimensional description of shape memory alloy thermomechanical behavior including plasticity. *Journal of the Brazilian Society of Mechanical Sciences and Engineering* 38(5): 1451–1472.
- Oliveira SDA, Dornelas VM, Savi MA, et al. (2018) A phenomenological description of shape memory alloy transformation induced plasticity. *Meccanica* 53: 2503–2523.
- Paiva A and Savi MA (2006) An overview of constitutive models for shape memory alloys. *Mathematical Problems in Engineering* 2006: 1–30.
- Patil D and Song G (2017) A review of shape memory material's applications in the offshore oil and gas industry. *Smart Materials and Structures* 26(9): 093002.
- Phillips FR, Wheeler RW, Geltmacher AB, et al. (2019) Evolution of internal damage during actuation fatigue in shape memory alloys. *International Journal of Fatigue* 124: 315–327.
- Preisach F (1935) Über die magnetische Nachwirkung [About the magnetic aftereffect]. *Zeitschrift für Physik* 94: 277–302.
- Rao A, Ruimi A and Srinivasa AR (2014) Internal loops in superelastic shape memory alloy wires under torsion-experiments and simulations/predictions. *International Journal of Solids and Structures* 51, 25–26: 4554–4571.
- Rao A and Srinivasa AR (2013) A two species thermodynamic Preisach model for the torsional response of shape memory alloy wires and springs under superelastic conditions. *International Journal of Solids and Structures* 50(6): 887–898.
- Rao Z, Leng J, Yan Z, et al. (2023) A three-dimensional constitutive model for shape memory alloy considering transformation-induced plasticity, two-way shape memory effect, plastic yield and tension-compression asymmetry. *European Journal of Mechanics - A/Solids* 99: 104945.
- Rizzello G, Mandolino MA, Schmidt M, et al. (2018) An accurate dynamic model for polycrystalline shape memory alloy wire actuators and sensors. *Smart Materials and Structures* 28: 025020.
- Ruth DJS, Sohn JW, Dhanalakshmi K, et al. (2022) Control aspects of shape memory alloys in robotics applications: A review over the last decade. *Sensors* 22(13): 4860.
- Scalet G, Karakalas A, Xu L, et al. (2021) Finite strain constitutive modelling of shape memory alloys considering partial phase transformation with transformation-induced plasticity. *Shape Memory and Superelasticity* 7(2): 206–221.

- Semenov ME, Borzunov SV, Meleshenko PA, et al. (2024) The Preisach model of hysteresis: Fundamentals and applications. *Physica Scripta* 99(6): 062008.
- Shreekrishna S, Nachimuthu R and Nair VS (2022) A review on shape memory alloys and their prominence in automotive technology. *Journal of Intelligent Material Systems and Structures* 34: 499–526.
- Smith RC (2005) *Smart Material Systems: Model Development*. Philadelphia: Society for Industrial and Applied Mathematics, SIAM.
- Song G, Zhao J, Zhou X, et al. (2005) Tracking control of a piezoceramic actuator with hysteresis compensation using inverse Preisach model. *IEEE/ASME Transactions on Mechatronics* 10(2): 198–209.
- Sordon F, El Khatib O, Courant R, et al. (2024) A novel scale-bridging method for MSMA linking continuum thermodynamics constitutive formulations to lumped system-level models. *Smart Materials and Structures* 33: 095014.
- Sreekumar M, Nagarajan T, Singaperumal M, et al. (2007) Critical review of current trends in shape memory alloy actuators for intelligent robots. *Industrial Robot An International Journal* 34(4): 285–294.
- Sun Y, Ma H, Li Y, et al. (2024) A novel rate-dependent direct inverse Preisach model with input iteration for hysteresis compensation of piezoelectric actuators. *International Journal of Control Automation and Systems* 22: 1277–1288.
- Trapanese M, Franzitta V and Viola A (2014) A dynamic model for hysteresis in magnetostrictive devices. *Journal of Applied Physics* 115(17): 17D141.
- Vasquez-Beltran MA, Jayawardhana B and Peletier R (2021) On the characterization of butterfly and multiloop hysteresis behavior. *IEEE Transactions on Automatic Control* 67(7): 3494–3506.
- Wang J, Gu X, Xu Y, et al. (2021) Thermomechanical modeling of nonlinear internal hysteresis due to incomplete phase transformation in pseudoelastic shape memory alloys. *Nonlinear Dynamics* 103, 2: 1393–1414.
- Wang SY, Zhan L, Bruhns OT, et al. (2022) Accurately and automatically simulating hysteresis loops of shape memory alloys. *Continuum Mechanics and Thermodynamics* 34(3): 739–761.
- Wang YF, Su CY, Hong H, et al. (2007) Modeling and compensation for hysteresis of shape memory alloy actuators with the Preisach representation. In: *2007 IEEE international conference on control and automation*, pp.239–244.
- Xue Z, Li L, Ichchou MN, et al. (2017) Hysteresis and the nonlinear equivalent piezoelectric coefficient of MFCs for actuation. *Chinese Journal of Aeronautics* 30(1): 88–98.
- Yamauchi K, Ohkata I, Tsuchiya K, et al. (2011) *Shape Memory and Superelastic Alloys: Applications and Technologies*. Cambridge: Woodhead Publishing.
- Young B, Orrostieta R, Haghgouyan B, et al. (2024) Fracture toughness and fatigue crack growth resistance of precipitate-free and precipitation hardened NiTiHf shape memory alloys. *Materials Science and Engineering A* 900: 146443.